AGU PUBLICATIONS

JGR

Journal of Geophysical Research: Solid Earth

RESEARCH ARTICLE

10.1002/2016JB013811

Key Points:
- We found the MgO, Pt, and Au scales which are consistent within ±1 GPa at 40-140 GPa and 300-2500 K
- We identified a larger discrepancy (±1 GPa) between the scales at 20-40 GPa and high temperature
- We constrained tightly the Clapeyron slopes of the postspinel and postperovskite boundaries

Supporting Information:
- Supporting Information S1
- Data Set S1
- Data Set S2
- Data Set S3
- Data Set S4

Correspondence to:
S.-H. Shim,
SHDShim@asu.edu

Citation:
Ye, Y., V. Prakapenka, Y. Meng, and S.-H. Shim (2017), Intercomparison of the gold, platinum, and MgO pressure scales up to 140 GPa and 2500 K, *J. Geophys. Res. Solid Earth*, *122*, 3450–3464, doi:10.1002/2016JB013811.

Received 2 DEC 2016
Accepted 28 APR 2017
Accepted article online 2 MAY 2017
Published online 13 MAY 2017
Corrected 22 MAY 2017

This article was corrected on 22 MAY 2017. See the end of the full text for details.

Intercomparison of the gold, platinum, and MgO pressure scales up to 140 GPa and 2500 K

Y. Ye[1,2], V. Prakapenka[3], Y. Meng[4], and S.-H. Shim[2]

[1]State Key Laboratory of Geological Processes and Mineral Resources, China University of Geosciences, Wuhan, China, [2]School of Earth and Space Exploration, Arizona State University, Tempe, Arizona, USA, [3]GSECARS, University of Chicago, Chicago, Illinois, USA, [4]Carnegie Institute of Washington, Washington, District of Columbia, USA

Abstract In order to intercalibrate the equations of state (EOSs) of the three widely used pressure standards, gold, platinum, and MgO, we have measured their unit cell volumes together in the laser-heated diamond anvil cell up to 140 GPa and 2500 K. At 300 K, three standards agree with each other within ±2.5 GPa to 135 GPa if the EOSs measured in quasi-hydrostatic media are used. We further refined the EOSs at 300 K, making them consistent with each other within ±1 GPa up to 135 GPa. At high temperature (T), the three standards match the best within ±1 GPa between 40 and 140 GPa, when we use the scales by Dorogokupets and Dewaele (2007). However, a 2–3 GPa discrepancy remains at 20–40 GPa and 1500–2000 K, with gold yielding the highest pressure (P). The pressure discrepancy is likely related to steep decreases in the Grüneisen parameter, the anharmonicity, and/or the electronic effects for the standards at the P-T conditions. Because gold melts near the temperatures expected for the mantle transition zone, severe anharmonic effects expected under premelting conditions make gold unsuitable for determining the phase boundaries in the region. The pressure scales by Dorogokupets and Dewaele (2007) provide tighter constrains on the Clapeyron slopes of the postspinel boundary to −2.0 to −2.7 MPa/K and the postperovskite boundary to 7–10 MPa/K. The data and refined EOSs presented here allow for reliable comparisons among experiments with different pressure standards for the entire P-T conditions expected for the Earth's lower mantle.

1. Introduction

Accurate pressure scales are essential in relating laboratory experiments to the geophysical observations of Earth and planetary interiors. Numerous efforts have been made to improve the pressure scales to a required level for meaningful comparisons for Earth science problems (~1 GPa or ~30 km in depth). Because the equations of state (EOSs) of Au, Pt, and MgO have been used extensively in laser-heated diamond anvil cell (LHDAC) and multianvil press studies to determine pressure during heating, many studies have been conducted on these three pressure standards, including experiments, modeling, and theory [e.g., *Zha et al.*, 2000; *Speziale et al.*, 2001; *Shim et al.*, 2002; *Tsuchiya and Kawamura*, 2002; *Tsuchiya*, 2003; *Dewaele et al.*, 2004; *Fei et al.*, 2007; *Dorogokupets and Dewaele*, 2007; *Dorogokupets and Oganov*, 2007; *Wu et al.*, 2008; *Tange et al.*, 2009; *Yokoo et al.*, 2009; *Dorfman et al.*, 2012; *Sokolova et al.*, 2013; *Dorogokupets et al.*, 2015].

Despite the numerous efforts, studies have still reported significant differences between these standards at high pressure (P) and temperature (T) [e.g., *Hirose et al.*, 2006a; *Shim*, 2008; *Ye et al.*, 2014]. While elasticity and shock wave measurements can provide absolute pressure scales, their applications have been limited to a few materials at limited P-T ranges and some additional data are required for the analysis [*Zha et al.*, 2000; *Li et al.*, 2006; *Tange et al.*, 2009; *Yokoo et al.*, 2009; *Kono et al.*, 2010; *Zhuravlev et al.*, 2013]. Although it does not provide absolute scales, intercomparison of the pressure standards provides important information on their accuracies and reconciles discrepancies between experimental results based on different pressure scales.

For example, *Dewaele et al.* [2004] and *Dorfman et al.* [2012] have compared many different pressure scales to very high pressure under low-deviatoric stress conditions. The studies have dramatically improved the 300 K isotherms of the widely used pressure standards, because they allow models to further refine the P-V-T EOSs using a wide range of data sets, including shockwave and 1 bar thermal measurements [e.g., *Dorogokupets and Dewaele*, 2007; *Tange et al.*, 2009; *Dorogokupets et al.*, 2015]. However, these data sets were measured only at 300 K. Although some data have been reported for comparing Au, Pt, and MgO at in situ high P-T

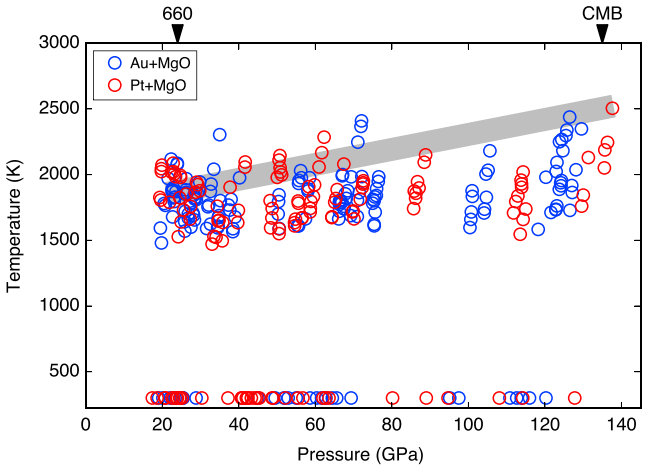

Figure 1. Pressure-temperature conditions of our experiments on the Au+MgO mixtures (blue circles) and the Pt+MgO mixtures (red circles). The gray line represents the mantle geotherm by *Brown and Shankland* [1981]. The pressures are calculated using the MgO scale by *Dorogokupets and Dewaele* [2007].

[*Dewaele et al.*, 2000; *Fei et al.*, 2004a; *Hirose et al.*, 2008; *Fei et al.*, 2007], the pressure ranges are limited. To our knowledge, no study so far tested the consistencies between all the three pressure standards for the entire pressure range of the lower mantle at the temperatures expected in the region.

In this paper, we report the measurements of the unit cell volumes of Au, Pt, and MgO at high *P-T* conditions up to 140 GPa and 2500 K, covering the expected *P-T* conditions of the lower mantle (Figure 1). The simultaneous measurements of Au+MgO and Pt+MgO allow us to compare the EOSs of Au, Pt, and MgO directly at high *P-T* and further refine them for consistency. We also apply our new results for reconciling discrepancies in the properties of the mantle phase boundaries.

2. Experimental Methods

We dried MgO powder (from Aldrich, purity of >99.999%) above 800 K for 24 h and then mixed with 10 wt % Pt (from Aldrich, purity of >99.9%, grain size of 0.5–1.2 μm) for the Pt+MgO sample and Au (from Aldrich, purity of >99.9%, grain size of 1.5–2.0 μm) for the Au+MgO sample. We did not mix Pt and Au directly, in order to avoid possible alloying between the metals during laser heating. For each mixture of Pt+MgO and Au+MgO, we prepared five different loadings in the symmetric-type diamond anvil cells (DACs). We provided experimental details in Table S1 in the supporting information [*Singh*, 1993; *Singh et al.*, 1998; *Singh and Takemura*, 2001; *Golding et al.*, 1967; *Menéndez-Proupin and Singh*, 2007; *Karki and Stixrude*, 1999].

For each DAC loading, we preindented a Re gasket to a thickness of 20–30 μm with a hole diameter of ~70% of the culet diameter. In the hole, we loaded a cold-pressed thin foil of a mixture (a thickness of ~10 μm and a diameter of 40–120 μm) with three or four MgO spacer particles (<10 μm) on each side of the culet for the purposes of propping up the foil during gas loading, to form insulating layers separating the foil from the diamond anvils for thermal insulation during laser heating. We also loaded a small ruby chip for pressure measurements during gas loading. The ruby chip was loaded near the edge of the sample chamber in order to prevent any chemical reaction with the pressure standards (Au, Pt, and MgO). We loaded Ar or Ne as a quasi-hydrostatic pressure medium. We cryogenically loaded liquid Ar into DAC below 10 GPa at Arizona State University. We loaded Ne gas for experiments at pressures higher than 35 GPa using the COMPRES-GSECARS high-pressure gas loading system [*Rivers et al.*, 2008].

We measured synchrotron X-ray diffraction (XRD) for the samples in LHDAC at in situ high *P-T* at beamline 13-IDD of the GeoSoilEnviroConsortium for Advanced Radiation Sources (GSECARS) sector (a wavelength of 0.3344 Å; a beam size of 3×4 μm^2) [*Prakapenka et al.*, 2008] and beamline 16-IDB of the High Pressure Collaborative Access Team (HPCAT) sector (a wavelength of 0.3515 Å; a beam size of 5×6 μm) [*Meng et al.*, 2006]. We increased the pressure of the samples in DAC to target pressures at room temperature and conducted laser heating. Near-infrared laser beams were focused on both sides of the sample in DAC. We aligned the laser beams coaxially with the X-ray beam, in order to measure diffraction patterns at the center of the heated spots. We conducted heating for more than 10 min, with a hot spot diameter of 25 μm.

In order to anneal deviatoric stresses, we heated the samples for 10 min at temperatures above 1900 K. For the EOS comparison, we use only the diffraction patterns measured after the 10 min of laser heating. The data include diffraction patterns at 1600–2500 K and room temperature, at high pressure. We measured the thermal radiation spectra from both sides of the sample using an imaging spectrometer. We fitted the spectra to the Planck gray body equation. Four to six different temperatures were measured during acquisition of an XRD pattern. We averaged the measurements and used the standard deviation for the 1σ uncertainty of the

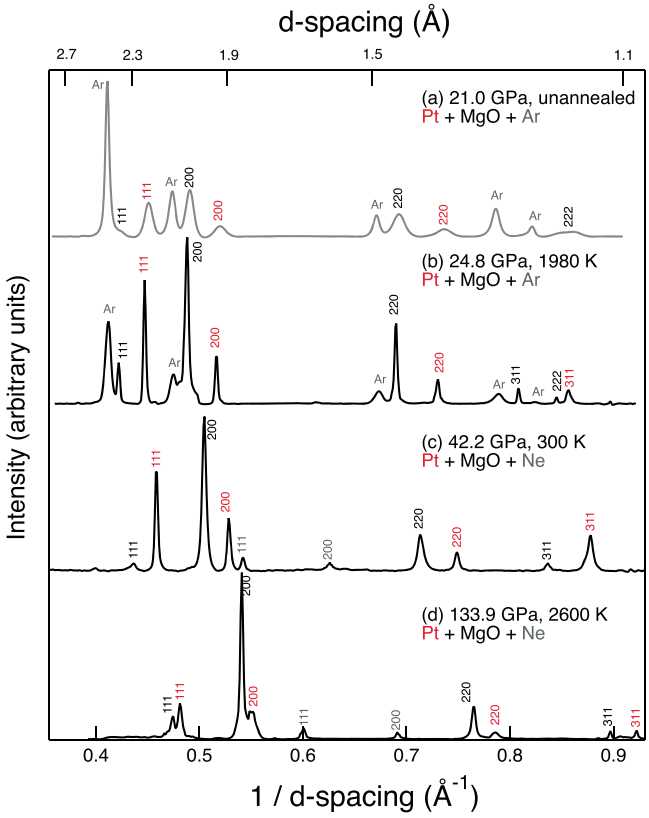

Figure 2. X-ray diffraction patterns of the Pt+MgO mixtures. The background was subtracted. The peaks labeled with black, red, and gray indices are from MgO, Pt, and Ne (or Ar), respectively. The pressure was calculated from the MgO scale by *Dorogokupets and Dewaele* [2007].

measured temperature. We measured 300 K XRD patterns from laser-heated spots. We obtained 1-D diffraction patterns from 2-D diffraction images using the software package fit2D [*Hammersley*, 1997] and fitted the diffraction peaks with pseudo-Voigt profile functions.

3. Results

3.1. Diffraction Observations and Stress Conditions

We measured four lines of Pt (111, 200, 220, and 311), five lines of Au (111, 200, 220, 311, and 222), and five lines of MgO (111, 200, 220, 311, and 222) in the diffraction patterns (Figures 2 and 3). We calculated the unit cell volumes by including all the diffraction peaks which are not severely overlapped and are sufficiently intense. For example, we did not include the Au 200 line and the MgO 200 line above 40 GPa, because of their severe overlap (Figure 3). The unit cell volumes obtained from the two beamlines (GSECARS and HPCAT) agree well with each other.

Although the diffraction images show continuous intensities of diffraction rings before heating, the diffraction rings become spotty after heating, suggesting sufficient heating for the recrystallization and the annealing of deviatoric stresses. In the 1-D patterns, the diffraction line widths decrease significantly with heating (Figures 2 and 3). The full width at half maxima (FWHM) of the Pt, Au, and MgO lines (111, 200, 220, 311, and 222) range between 3 and 11×10^{-3} for $\Delta2\theta/2\theta$, while our values without laser annealing are much greater ($20-30\times10^{-3}$) (Figure S1). We found no significant difference in peak width between runs with Ar (15–30 GPa) and Ne (30–125 GPa) (Figure S1).

The width of diffraction peaks depends on (1) instrumental resolution, (2) grain size, and (3) microstresses. Therefore, it is difficult to compare our values with other studies. Nevertheless, our $\Delta2\theta/2\theta$ values are similar to those reported for an Au foil ($2-8\times10^{-3}$) and a powder ($4-20\times10^{-3}$) compressed in a He medium [*Takemura and Dewaele*, 2008]. Our values are also smaller than that reported for a Pt powder ($17-32\times10^{-3}$) compressed in a He or Ne medium in *Dorfman et al.* [2012]. In some previous studies on Au and Pt, the normalized FWHM for 200 is systematically larger than that for 111, and generally increases with an increase in pressure [*Takemura and Dewaele*, 2008; *Dorfman et al.*, 2012], because the differential stress makes the 200 diffraction peaks broaden selectively with pressure [*Takemura*, 2001]. However, in our study, the widths of the 200 lines remain similar to those of the 111 lines up to our maximum pressure.

Similar to *Takemura and Dewaele* [2008] and *Dorfman et al.* [2012], we estimated the uniaxial stress parameters, *t*, for Pt and Au (Figure S2). Our *t* values range between −0.5 and 1 GPa for both Pt and Au at 17–126 GPa and 300 K. The magnitude of the estimated uniaxial stress is comparable to the uncertainties in pressure for Pt and Au. Our *t* values are similar to those for Au in a He medium (<1 GPa) in *Takemura and Dewaele* [2008], but smaller than those for Pt in a He/Ne medium (1–4 GPa, without laser annealing) in *Dorfman et al.* [2012]. Our *t* values for Pt is similar to *Dorfman et al.* [2012] in a NaCl medium with laser annealing. Because of severe peak overlaps, particularly the weak 111 peak, and very small elastic anisotropy [*Zha et al.*, 2000], we could not calculate the *t* of MgO reliably through the same method.

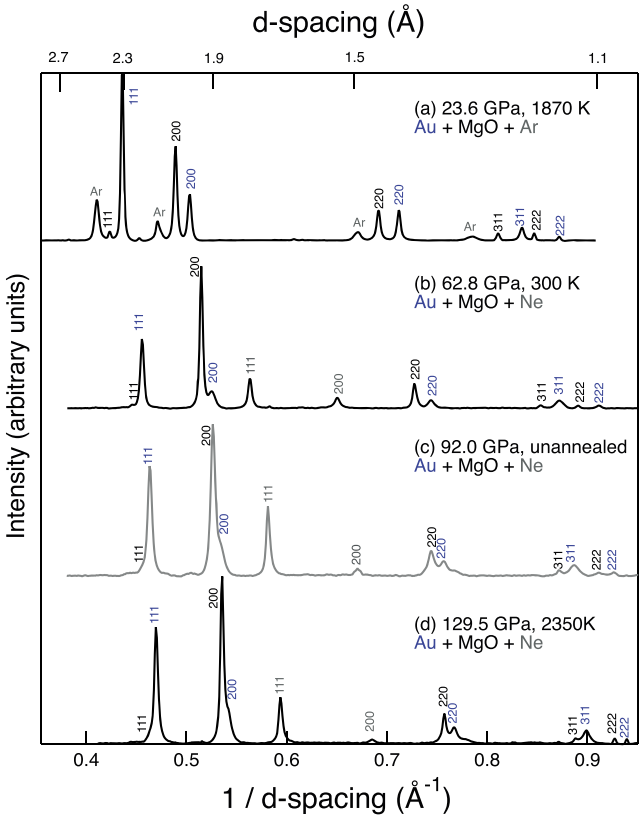

Figure 3. X-ray diffraction patterns of the Au+MgO mixtures. The background was subtracted. The peaks labeled with black, blue, and gray indices are from MgO, Au, and Ne (or Ar), respectively. The pressure was calculated from the MgO scale by *Dorogokupets and Dewaele* [2007].

Because of the volumetric dominance (~95%) in our cold-compressed sample foils, the mechanical properties of MgO, which has the highest shear strength among the three materials, may affect the stress field for Pt and Au, while MgO itself would be affected by the stress field controlled by Ne or Ar. Although MgO may support more deviatoric stresses than Au and Pt, even in the non-hydrostatic conditions without a pressure medium, it may support up to 5 GPa of shear stress at 130 GPa and 300 K according to *Duffy et al.* [1995]. Because MgO is surrounded by either a Ne or Ar medium and thermally annealed to 2000 K in our experiments, the shear stress supported by MgO should be lower for our data at 300 K. *Weidner et al.* [1994] found that the differential yield strength of MgO decreases dramatically from ~3 GPa to ~0.1 GPa by heating from 300 K to 1300 K at 8 GPa. Therefore, deviatoric stress for our high-temperature data at $T \geq 1600$ K would be even lower than that for our 300 K data.

We cold compressed MgO+metal powder mixtures to 2–3 GPa in DAC to make foils for loading in LHDAC. However, we found that the foils break easily before and after experiments. Our microscope observations showed that the foils contain cracks and pores. Therefore, at high pressure, Ne or Ar, which is used as a pressure medium, should have penetrated through the cracks and grain boundaries and even surround some grains. Therefore, the stress field for Pt, Au, and MgO grains in our experiments is controlled by the mechanical properties of both MgO and the soft pressure medium (Ne or Ar). We also calculated pressures from the individual diffraction lines of Au, Pt, and MgO, as all of them have cubic structures. We found that majority of our data points have the pressure difference less than 2 GPa. We excluded a few data points which show the pressure difference greater than 2 GPa. The rejected data points do not represent more than 5% of the total number of the data points. We provide full data sets for the unit cell volume measurements in the supporting information (Data Sets S1–S4).

3.2. Comparison of Pressure Scales at 300 K and High Pressure

In order to make comparisons between the existing pressure scales, data sets should have sufficiently low data scatter. The level of data scatter in our 300 K data sets (Pt+MgO and Au+MgO) is ±1 GPa, which provides us with 1 GPa resolution for our comparison up to 135 GPa. *Dorfman et al.* [2012] conducted measurements on a number of pressure standards, including the ones we studied here (MgO, Pt, and Au), up to 220 GPa at 300 K. While the study measured Pt and MgO together, they did not measure Au and MgO directly. Therefore, we compare our Pt+MgO data with their data (Figure S3). At our pressure range, some data points in *Dorfman et al.* [2012] agree with our data. Although our pressure coverage is roughly half of that by *Dorfman et al.* [2012], our data show smaller scatter.

A few studies have reported EOSs of all three pressure standards using the same (or similar) formalisms and data reduction methods. Adopting the *P-V* data at 300 K by *Dewaele et al.* [2004], *Fei et al.* [2007] constructed *P-V-T* EOSs of some pressure standards, including Au and Pt (Au-F07 and Pt-F07) through the Mie-Grüneisen-Debye approach. Although it is based on an independent data set, *Speziale et al.* [2001] constructed an MgO scale (MgO-S01) based on a similar EOS formalism except for the modified volume dependence of

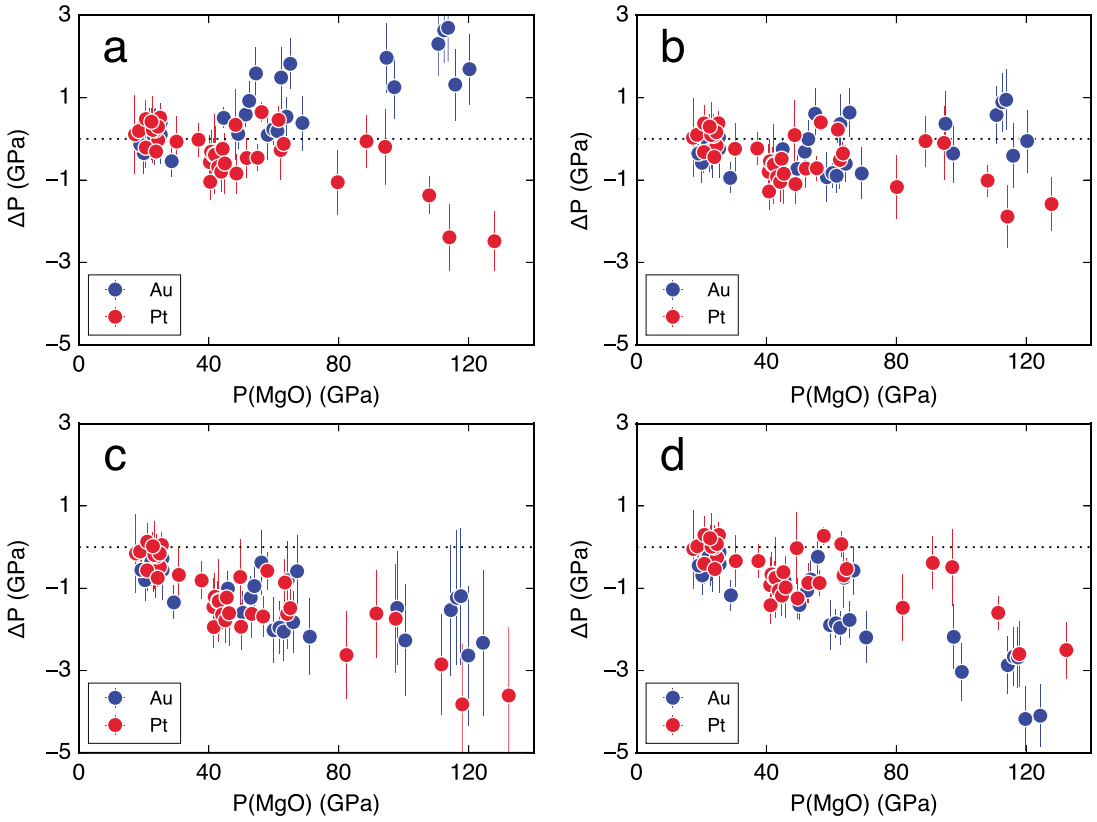

Figure 4. Differences in pressure among the Pt (red), Au (blue), and MgO (dashed lines at 0) scales at 300 K and high pressure. (a) Au-F07, Pt-F07, and MgO-S01; (b) Au-, Pt-, and MgO-D07; (c) Au-Y09, Pt-Y09, and MgO-T09; and (d) Au-, Pt-, and MgO-D15. The error bars are the 1σ uncertainties estimated from the uncertainties in the measured unit cell volume and the uncertainties of the thermoelastic properties provided in the original papers.

the Grüneisen parameter. These three scales are all based on static compression in quasi-hydrostatic media for the materials [*Zha et al.*, 2000; *Dewaele et al.*, 2004]. Through our data, we found that these three scales are consistent with each other within ±2.5 GPa up to 140 GPa at 300 K (Figure 4a). However, these three scales show a diverging trend with an increase in pressure, where Au-F07 is higher, MgO-S01 is intermediate, and Pt-F01 is lower in pressure.

Dorogokupets and Dewaele [2007] used the same quasi-hydrostatic measurements [*Zha et al.*, 2000; *Dewaele et al.*, 2004] combined with shockwave and other thermal measurements to construct the EOSs based on the Mie-Gŕuneisen-Debye approach with the anharmonic and electronic terms. We found the best agreement between the three scales (Au-, Pt-, and MgO-D07) at 300 K within ±1.5 GPa. We found no systematic trends in the differences (Figure 4b). Using a different EOS formalism, *Dorogokupets et al.* [2015] updated their EOSs using the latest static compression data sets (Figure 4d). While Au-D15 and Pt-D15 [*Dorogokupets et al.*, 2015] agree well with each other, these scales show systematic differences with the MgO-D15 scale with an increase in pressure.

Tange et al. [2009] and *Yokoo et al.* [2009] have constructed the EOSs using shockwave data combined with some thermal data sets at 1 bar. The studies did not measure the 300 K isotherms of MgO, Au, and Pt directly. Instead, the 300 K isotherms were obtained through shockwave data reduction combined with the thermal properties of the standards measured at 1 bar. Our data show that the Au-Y09 and Pt-Y09 scales agree well with each other. However, similar to the scales by *Dorogokupets et al.* [2015], they show systematic differences with the MgO-T09 scale (Figure 4c).

3.3. Internally Consistent Pressure Scales for Pt, Au, and MgO at 300 K

While our data sets provide accurate comparison of the widely used pressure standards, Au, Pt, and MgO, they do not provide information on absolute pressure scales. Therefore, it remains uncertain which of the three pressure standards, or even which of the existing pressure scales, provide the most accurate pressure. Absolute pressures have been estimated through sound velocity measurements [e.g., *Zha et al.*, 2000; *Li et al.*, 2006;

Kono et al., 2010] and shockwave measurements [e.g., *Jamieson et al.*, 1982; *Duffy and Ahrens*, 1995; *Yokoo et al.*, 2009]. However, due to some limitations in these techniques (such as limited *P-T* range or uncertainties in temperature), it remains uncertain which of the existing scales is most accurate. Attemps have also been made to constrain the EOSs tightly through matching them to various different data sets [e.g., *Speziale et al.*, 2001; *Shim et al.*, 2002; *Dorogokupets and Dewaele*, 2007; *Tange et al.*, 2009].

As shown in the previous section, we found the best match among the pressure scales in *Dorogokupets and Dewaele* [2007]. *Dorogokupets and Dewaele* [2007] obtained their EOSs through the inversion of different data sets including shockwave. Their 300 K EOSs are consistent with the EOSs of Au and Pt [*Dewaele et al.*, 2004], where the shockwave-reduced isotherms of several standards are compared under quasi-hydrostatic stress conditions at 300 K. Their MgO scale is also consistent with an absolute pressure scale through Brillouin measurements by *Zha et al.* [2000]. Therefore, we decided to further refine the EOSs of Au, Pt, and MgO using *Dorogokupets and Dewaele*, 2007's [2007] scales as starting models. In this refinement, our new data allow us to compare the EOSs of all the three pressure standards directly in internally consistent fashion.

We conducted a series of EOS fittings for our data sets by taking different materials as pressure standards. For MgO, because we have both Pt+MgO and Au+MgO data sets, we can set MgO as a pressure standard to fit the EOSs of Au and Pt. For Pt (or Au), we first take Pt (or Au) as a pressure standard and fit the EOS of MgO using our Pt+MgO (or Au+MgO) data. Then we use the fitted EOS of MgO based on Pt (or Au) as a pressure scale and fit the EOS of Au (or Pt) using our Au+MgO (or Pt+MgO) data set. In this way, we can construct robust pressure scales for Au, Pt, and MgO, which are consistent with each other up to 135 GPa and 300 K.

The results are presented in Table 1 together with 300 K EOSs reported by other studies. In our fits, we fixed K_0 and V_0 to the values reported in *Dorogokupets and Dewaele* [2007] and refined K_0' in the Vinet equation [*Vinet et al.*, 1987]. We obtained $K_0' = 4.10-4.18$ for MgO, $K_0' = 5.81-5.90$ for Au, and $K_0' = 5.23$ for Pt (Figures 5–7). The values are consistent with *Dorogokupets and Dewaele* [2007], numerically proving that three scales from the study are already consistent with each other. Our values are within the range reported for these three standards in the literature. The most important advantage of our fitting results is that all three scales, MgO, Pt, and Au, are consistent with each other up to 135 GPa within ±1 GPa which is based on the random scatter in the fit residue (Figures 5–7).

3.4. Comparison of Pressure Scales at High Temperature and High Pressure

Our high-temperature data were obtained between 1600 and 2500 K at high pressures up to 140 GPa, allowing for the intercomparison of the Pt, Au, and MgO scales at the entire *P-T* conditions expected for the Earth's lower mantle (Figure 1). As shown in Figure 8, after correcting temperature differences between data points, the data scatter for individual pressure scales is less than ±1 GPa, comparable to that in our 300 K data sets. Again, this allows us to make high-precision comparison between the pressure scales at high *P-T*.

Our data indicate that the Au-F07, Pt-F07, and MgO-S01 scales agree with each other within ±4 GPa but with systematic differences (Figure 8a). Pt-F07 is the lowest in pressure among the all three scales. The Au-F07 scale yields systematically higher pressures throughout our pressure range. The differences were the largest at 20–40 GPa and 120–140 GPa. We found the best agreement among the three standards when the EOSs by *Dorogokupets and Dewaele* [2007] are used (Figure 8b). All three scales are in agreement within ±1 GPa between 40 and 125 GPa. However, the differences are noticeably larger at 20–30 and 130–140 GPa, except for two outlier data points at ~130 GPa.

When the scales by *Yokoo et al.* [2009], *Tange et al.* [2009], and *Dorogokupets et al.* [2015] were used, we found systematic differences with larger magnitudes (Figures 8c and 8d). In these two cases, the Au and Pt scales are in reasonable agreement. However, the MgO scales are significantly different from the other two standards. The discrepancies among pressure standards in these studies show similar patterns as those found at 300 K (Figure 4), suggesting that the disagreement in their 300 K isotherms is affecting the high *T* EOSs for some degree. Another noticeable trend is that the discrepancy among the three pressure standards at 20–30 GPa range persists throughout all the comparisons we made in Figure 8. At this pressure range, the 300 K isotherms are in agreement (Figure 4). Therefore, the mismatch should result from the thermal parts of the EOSs.

3.5. Source of the Discrepancy in Thermal EOSs of the Pressure Standards

Because the pressure scales have been constructed to fit both high-pressure and low-pressure data and EOSs normally take 1 bar as a reference condition (because high-quality measurements exist at the condition), it is

Table 1. Equations of State of MgO, Gold, and Platinum at 300 K[a]

Method	References	K_0 (GPa)	K_0'	Equation	Scales
		MgO			
Shock	*Jamieson et al.* [1982]	160	4.4	Vinet	
Ultrasonics	*Li et al.* [2006]	161.3	4.24	BM	
	Kono et al. [2010]	160.9	4.35	BM	
Theory	*Wu et al.* [2008]	160	4.23	BM	
XRD	*Dewaele et al.* [2000]	161	4.01	Vinet	
Others	*Speziale et al.* [2001]	160.2	3.99	BM	
	Dorogokupets and Dewaele [2007]	160.3	4.18	Vinet	
	Kennett and Jackson [2009]	160.34	4.34	BM	
	Tange et al. [2009]	160.6	4.37	Vinet	
	Dorogokupets et al. [2015]	160.3	4.25	Kunc	
XRD	This study	160.3	4.182(19)	Vinet	Au-D07
		160.3	4.109(22)	Vinet	Pt-D07
		Au			
Shock	*Jamieson et al.* [1982]	175.3	5.05	Vinet	
	Yokoo et al. [2009]	167.5	5.94	Vinet	
XRD	*Dewaele et al.* [2004]; *Fei et al.* [2007]	167	6	Vinet	
	Takemura and Dewaele [2008]	167	5.9	Vinet	
	Dorfman et al. [2012]	167	5.88	Vinet	
Theory	*Tsuchiya* [2003]	166.7	6.12	Vinet	
	Greeff and Graf [2004]	167.9	5.64	Vinet	
Others	*Shim et al.* [2002]	167	5	BM	
	Dorogokupets and Dewaele [2007]	167	5.9	Vinet	
	Dorogokupets et al. [2015]	167	5.9	Vinet	
XRD	This study	167	5.897(22)	Vinet	MgO-D07
		167	5.813(22)	Vinet	Pt-D07
		Pt			
Shock	*Holmes et al.* [1989]	266	5.81	Vinet	
	Yokoo et al. [2009]	276.4	5.48	Vinet	
XRD	*Dewaele et al.* [2004]; *Fei et al.* [2007]	277	5.08	Vinet	
	Zha et al. [2008]	273.5	4.7	BM	
	Dorfman et al. [2012]	277	5.43	Vinet	
Theory	*Matsui et al.* [2009]	273	5.2	Vinet	
	Ono et al. [2011]	290.8	5.11	BM	
Others	*Dorogokupets and Dewaele* [2007]	277.3	5.12	Vinet	
	Dorogokupets et al. [2015]	275	5.43	Vinet	
XRD	This study	277.3	5.230(33)	Vinet	Au-D07
		277.3	5.226(33)	Vinet	MgO-D07

[a]BM: Birch-Murnaghan equation.

surprising to find the persisting discrepancy among the Au, Pt, and MgO scales at our lowest-pressure range even for the best matched EOSs [*Dorogokupets and Dewaele*, 2007].

The widely used pressure scales we consider in this study are based on the Mie-Grüneisen approach:

$$P_{\mathrm{tot}}(V,T) = P_{\mathrm{st}}(V,T_{\mathrm{ref}}) + \Delta P_{\mathrm{th}}(V,T) + \Delta P_{\mathrm{el}}(V,T), \quad (1)$$

where the total pressure at given V and T (P_{tot}) is expressed as a sum of the static pressure (P_{st}) at a reference temperature (T_{ref}, normally 300 K), the thermal pressure (ΔP_{th}), and the electronic effects (ΔP_{el}). Because the 300 K isotherms of MgO, Au, and Pt are consistent with each other in *Dorogokupets and Dewaele* [2007] as

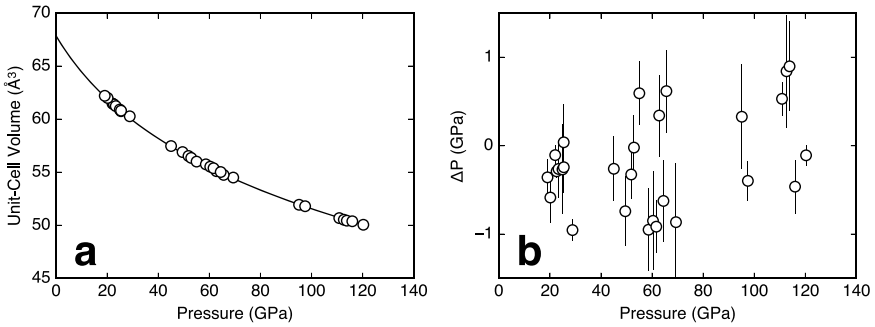

Figure 5. Equation of (a) state fit and (b) fit residue for Au at 300 K with MgO-D07 as a pressure scale. The error bars are the estimated 1σ uncertainties.

we showed (Figure 4), the discrepancy at 20–40 GPa must come from the nonstatic parts of the MgO, Pt, and Au EOSs, such as the thermal, electronic, and/or anharmonicity terms. The electronic effects are normally much smaller than the thermal pressure terms in Au and Pt [*Tsuchiya and Kawamura*, 2002; *Dorogokupets and Oganov*, 2007].

The key parameter in the thermal pressure is the Grüneisen parameter, γ. In previous studies, the Grüneisen parameter at 1 bar (γ_0) has been tightly constrained for Au, Pt, and MgO. However, its volume-dependent behavior has been uncertain as it is reflected by various different formalisms used in the literature. For example, *Fei et al.* [2007] used the following relation for Au and Pt:

$$\gamma = \gamma_0 \left(\frac{V}{V_0}\right)^q, \tag{2}$$

where q (the logarithmic volume dependence of γ) is assumed to be a constant.

For MgO, *Speziale et al.* [2001] found that the above relation does not fit the existing data well enough and introduced a new relation:

$$\gamma = \gamma_0 \exp\left\{\frac{q_0}{q_1}\left[\left(\frac{V}{V_0}\right)^{q_1} - 1\right]\right\}. \tag{3}$$

Later, *Dorogokupets and Dewaele* [2007] adopted the following relation:

$$\gamma = \gamma_\infty + (\gamma_0 - \gamma_\infty)\left(\frac{V}{V_0}\right)^\beta, \tag{4}$$

where γ_∞ is the Grüneisen parameter at infinite compression and β is a fitting parameter for the volume dependence. *Tange et al.* [2009] and *Yokoo et al.* [2009] used essentially the same formalism as equation (4). It is possible that the differences in these equations combined with different parameters used are responsible for the discrepancy we found at 20–40 GPa in all the scales we compared in this study. In order to explore

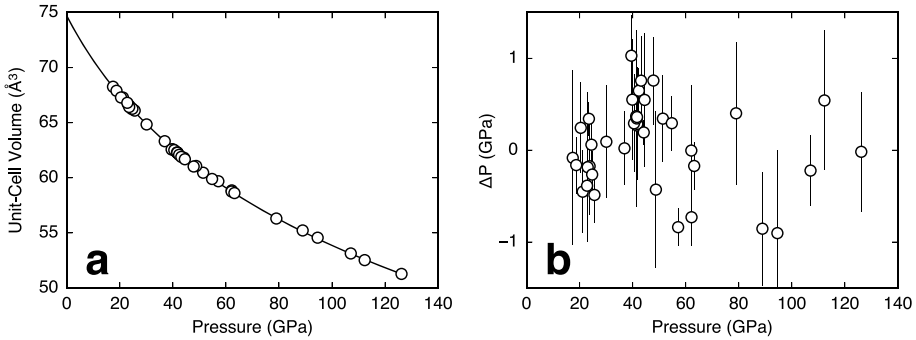

Figure 6. Equation of (a) state fit and (b) fit residue for MgO at 300 K with Pt-D07 as a pressure scale. The error bars are the estimated 1σ uncertainties.

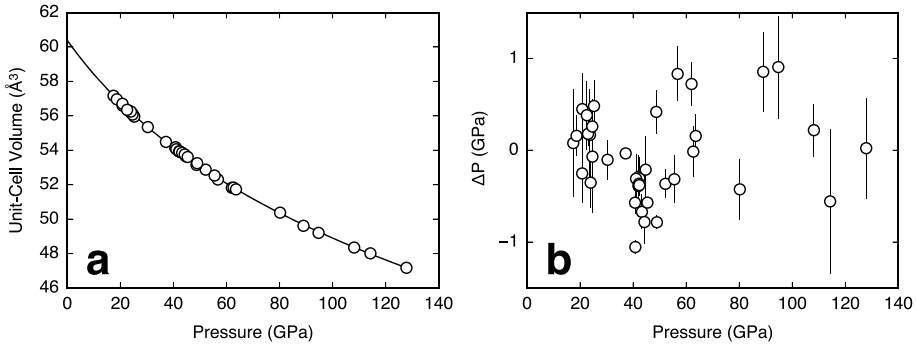

Figure 7. Equation of (a) state fit and (b) fit residue for Pt at 300 K with Au-D07 as a pressure scale. The error bars are the estimated 1σ uncertainties.

source of the discrepancy at 20–40 GPa and high temperature, we calculate the Grüneisen parameters and thermal pressures of the three pressure standards at 2000 K and high pressures in Figure 9. The pressures for the x axes in the figure are the total pressures ($P_{tot}(V, 2000K)$) in equation (1). $P_{2000K} - P_{300K}$ in Figures 9b, 9d, and 9f is thermal pressure between 2000 and 300 K, namely, $P_{tot}(V, 2000K) - P_{st}(V, 300K)$ ($= \Delta P_{th}(V, 2000K) + \Delta P_{el}(V, 2000K)$) in equation (1). For the Grüneisen paramater at 2000 K, γ_{2000K}, we found very steep changes in many EOSs for all three pressure standards we study between 0 and 40 GPa. Above 40 GPa at 2000 K, the change in the Grüneisen parameter is much smaller. The different formalisms of the pressure dependence (for example, between *Fei et al.* [2007] and *Dorogokupets and Dewaele* [2007]) results in very different behaviors of γ_{2000K} between 0 and 40 GPa for all three pressure standards we studied.

We also calculate pressure differences between 2000 and 300 K isotherms for given volumes, i.e., pressure contributions from nonstatic terms, $P_{tot}(V, 2000K) - P_{st}(V, 300K)$, in equation (1), including the thermal ($\Delta P_{th}(V, 2000K)$) and electronic ($\Delta P_{el}(V, 2000K)$) effects which are temperature sensitive. The scales by

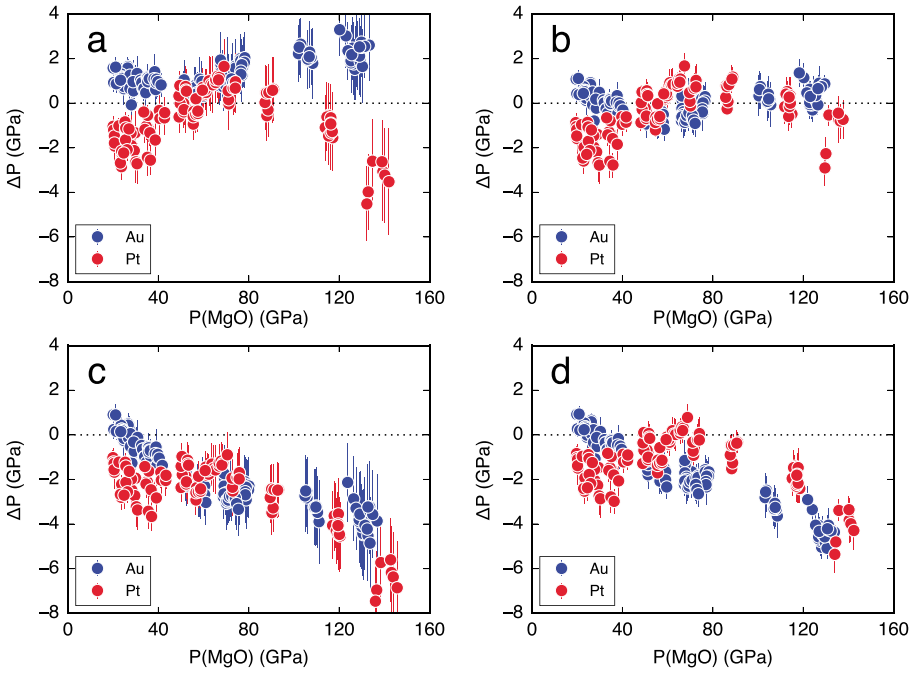

Figure 8. Differences in pressure among the Pt (red), Au (blue), and MgO (dashed lines at 0) scales at 1500–2500 K and high pressure. (a) Au-F07, Pt-F07, and MgO-S01; (b) Au-, Pt-, and MgO-D07; (c) Au-Y09, Pt-Y09; and MgO-T09; and (d) Au-, Pt-, and MgO-D15. The error bars are the 1σ uncertainties estimated from the uncertainties in measured properties (unit cell volume and temperature) and the uncertainties of the thermoelastic properties provided in the original papers.

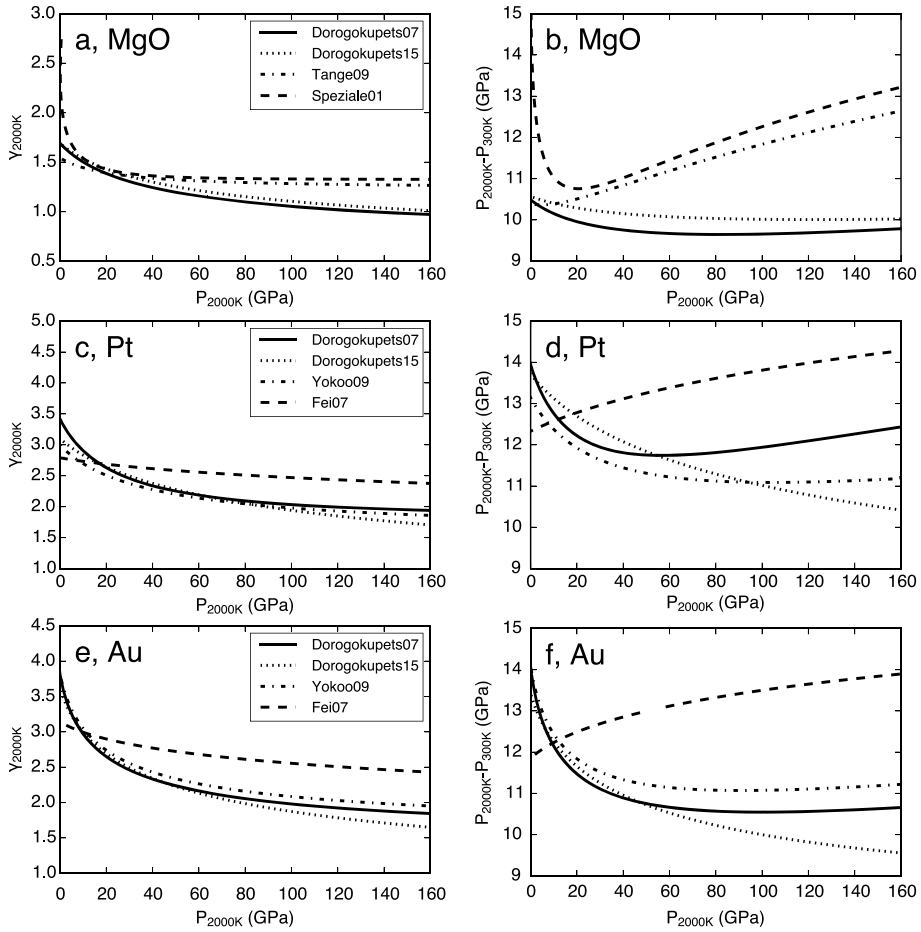

Figure 9. (a, c, and e) Grüneisen parameters, γ_{2000K}, and (b, d, and f) thermal pressures, $P_{tot}(V, 2000K) - P_{st}(V, 300K)$ $(= \Delta P_{th}(V, 2000K) + \Delta P_{el}(V, 2000K))$ in equation (1), of MgO, platinum, and gold at 2000 K and high pressure. Solid curves: *Dorogokupets and Dewaele* [2007], dotted curves: *Dorogokupets et al.* [2015], dashed dot curves: *Tange et al.* [2009] for MgO and *Yokoo et al.* [2009] for Pt and Au, and dashed curves: *Speziale et al.* [2001] for MgO and *Fei et al.* [2007] for Au and Pt.

Dorogokupets and Dewaele [2007] and *Dorogokupets et al.* [2015] include both the anharmonic effects (Au, Pt, and MgO) and the electronic effects (Au and Pt). The scales by *Yokoo et al.* [2009] and *Tange et al.* [2009] include the electronic effects for Au and Pt, but not the anharmonic effects.

We found steep changes in the nonstatic terms $(\Delta P_{th}(V, 2000K) + \Delta P_{el}(V, 2000K))$ between 0 and 40 GPa in many pressure scales. The magnitude of the steep change is 1–4 GPa which is similar to the observed discrepancies at the conditions. The rate of the change in the nonstatic effects is, in general, much less steep above 40 GPa. Figure 9 suggests that the main sources for the discrepancy between 20 and 40 GPa identified by our study could be from the volume dependence of Grüneisen parameter. Similar to the refinements we made for the 300 K data in the previous section, we set one of the three materials as a pressure standard and fit the EOSs of the other two standards at high temperature. We used the same EOSs [*Fei et al.*, 2007; *Dorogokupets and Dewaele*, 2007; *Speziale et al.*, 2001; *Tange et al.*, 2009; *Yokoo et al.*, 2009] for the refinement. We found that all the fittings require extremely steep changes in the nonstatic pressure terms, such as the Grüneisen, anharmonic, and/or electronic parameters, below 40 GPa. This difficulty likely suggests that it is not one of the three standards which have the problem in its EOS at the pressure range. Instead, it can be two or even all three standards which have the problem at the pressure range.

This low-pressure and high-temperature region may be challenging for the existing EOSs because the anharmonic and electronic effects change (likely decrease) rapidly with an increase in pressure and their magnitudes (2–4 GPa) remain still significant. In fact, the melting temperature of gold (e.g., 2200 K at 20 GPa) is very

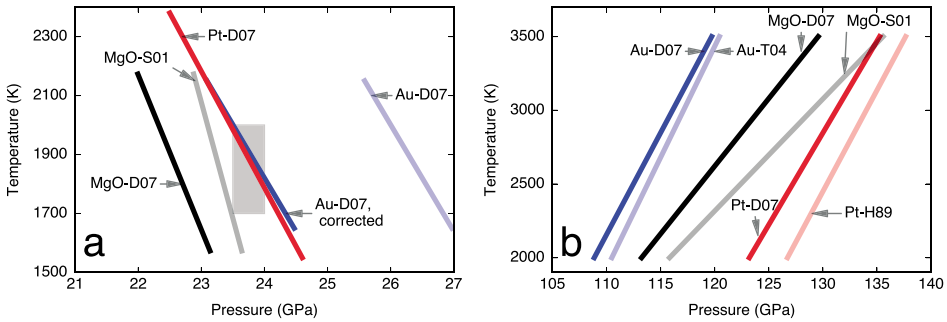

Figure 10. Mantle phase boundaries with different pressure scales: (a) the postspinel boundary (black solid line: *Fei et al.* [2004b] with the MgO-D07 scale; light blue line: *Ye et al.* [2014] with the Au-D07 scale; blue solid line: *Ye et al.* [2014] with the Au-D07 scale and −3 GPa correction; and red solid line: *Ye et al.* [2014] with the Pt-D07 scale) and (b) the postperovskite boundary (blue lines: *Hirose et al.* [2006b]; black lines: *Tateno et al.* [2009]; red lines: *Ono and Oganov* [2005]; solid lines: D07 scales; and light-colored lines: originally used scales).

close to the temperatures expected at the pressure in the mantle (i.e., the mantle transition zone) [*Errandonea*, 2013]. Considering the fact that anharmonic effects become particularly severe as temperature approaches melting and the melting temperature of gold is low at the pressure range, gold would not be a good choice as an internal pressure standard for measuring the phase boundaries in the mantle transition zone. Instead, because platinum (e.g., 2900 K at 20 GPa) and MgO (e.g., ≥3700 K at 20 GPa) have much higher melting temperatures [*Errandonea*, 2013; *Zhang and Fei*, 2008], the anharmonic effects, which are not currently modeled with sufficient accuracy, should be much less of an issue than gold. If the main source of the discrepancy at low pressure is the anharmonic effect, as discussed above, it would be important to have *P-V-T* data for a wide range of temperatures, because the term is sensitive to temperature. Because we designed our experiments for examining mutual consistency between the pressure standards for a wide range of pressures at the mantle-related temperatures, the temperature range is limited (1500–2000 K at 20–40 GPa) and therefore not suitable for constraining the anharmonic effects. Future studies should focus on obtaining high-resolution data for the elastic moduli for a wide range of temperature at 0–40 GPa. Theoretical investigations on anharmonic and electronic contributions at high pressure would be also very useful.

4. Implications for the Mantle Phase Boundaries

Numerous studies have been performed to understand the origins of the seismic discontinuities in the mantle. Accurate pressure scales have been the central issue for over a decade, since the controversy on the postspinel transition [*Irifune et al.*, 1998; *Shim et al.*, 2001]. The postspinel transition has been believed to be the origin of the globally observed seismic discontinuity at 660 km depth [*Bernal*, 1936]. The first in situ multianvil experiments [*Irifune et al.*, 1998] reported 2–3 GPa lower pressure of the transition than the pressure expected for the 660 km discontinuity (23–24 GPa at 1600–2000 K). A later LHDAC study [*Shim et al.*, 2001] suggested that the gold scale used in the multianvil study may underestimate pressure and if the Pt scale [*Holmes et al.*, 1989] is used, the postspinel transition pressure agrees well with the conditions expected for the 660 km discontinuity.

Although the gap has been reduced, later multianvil press studies with updated gold scales and MgO scales [*Litasov and Ohtani*, 2002; *Katsura et al.*, 2003; *Fei et al.*, 2004b] combined with energy-dispersive XRD have reported the boundary at systematically lower pressures than that for the 660 km discontinuity. *Ye et al.* [2014] have measured the postspinel boundary in different mantle-related compositions in LHDAC with high-resolution angle dispersive XRD, including pure Mg_2SiO_4 and pyrolite, and reported that the *P-T* conditions of the postspinel boundary agree well with those expected for the 660 km discontinuity if the platinum scales are used. However, they found that the gold scales systematically overestimate pressure by 3 GPa compared with the platinum scales.

As shown in Figure 10a, we obtained the best match between the postspinel transition pressure and the pressure expected for the 660 km depth (23–24 GPa) when the Pt-D07 scale is used. As reported by *Ye et al.* [2014], the Au-D07 scale predicts a 2–3 GPa higher pressure for the same phase boundary. As discussed above, due to the low melting temperature of gold, anharmonic effects could be severe for gold at the *P-T* conditions of the experiments. However, platinum has much higher melting temperature at the experimental pressures

and therefore the anharmonic effects should be much less severe. In many pressure scales, anharmonic effects are not included. Even if included, as discussed in the previous section, it appears that the correction is not sufficient. Therefore, the most reasonable choice for the pressure scale in this case would be platinum rather than gold. We take into account the pressure difference between the Pt and Au scales based on our new data reported here and correct the pressure difference from the boundary measurements by *Ye et al.* [2014] such that the Au scale matches with the Pt scale (the solid blue line in Figure 10). With the correction, we found an excellent agreement for both results with the pressure expected for the 660 km discontinuity.

Although our study suggests that the MgO scale overpredicts pressure compared with the Pt scale at this pressure range (Figure 8), a multianvil study [*Fei et al.*, 2004a] with the MgO scale reported lower pressures for the postspinel boundary than the boundary from LHDAC using the Pt scale, which appears to be inconsistent with our finding here. As shown above, because the thermal contribution to the total pressure rapidly decreases at the pressure range (20–40 GPa) in the MgO, Pt, and Au scales, the impact of uncertainties in volume measurements for pressure standards would be, in fact, much larger than the impact at higher pressures. Therefore, it is important to ensure the accurate measurements of the unit cell volumes of pressure standards with as many diffraction lines as possible.

The reported Clapeyron slope of the postspinel boundary in some multianvil press studies has been systematically lower (−0.4 to −1.4 MPa/K) [*Katsura et al.*, 2003; *Fei et al.*, 2004b] than seismic estimations for the 660 discontinuity [*Lebedev et al.*, 2002]. However, *Shim et al.* [2001] and *Ye et al.* [2014] have reported a Clapeyron slope of the postspinel boundary consistent with those of the 660 km discontinuity using the Pt and Au scales, −2.5 to −3.0 MPa/K.

If we use the MgO-D07 scale for the multianvil data by *Fei et al.* [2004a], it increases the Clapeyron slope to −1.9 MPa/K, reducing the discrepancy with the LHDAC studies and seismic estimations. The slope was formerly estimated to be much lower in −1.37 MPa/K using the MgO-S01 scale. The corrected value is in better agreement with the seismic estimation for the 660 km discontinuity [*Lebedev et al.*, 2002], −3 MPa/K.

While it is tempting to calibrate the Au and MgO scales with respect to the Pt scale, because it provides the best match between the postspinel boundary and the 660 km discontinuity, this requires an assumption that the postspinel transition is responsible for the 660 km discontinuity. On the other hand, MgO has been regarded as an ideal material as a pressure standard [*Oganov and Dorogokupets*, 2003; *Wu et al.*, 2008]. However, our comparison reveals that the MgO scales overestimate pressure with respect to the Pt scale which yields consistent pressure for the LHDAC data with the 660 km discontinuity.

Because *Dorogokupets and Dewaele* [2007]'s EOSs of all three pressure standards agree with each other well at the *P-T* conditions expected for the core-mantle boundary, we corrected the results from different studies on the postperovskite transition with respect to the scales. However, we found that such correction cannot completely resolve the existing discrepancies for the depth, although the correction reduces the disagreement (Figure 10b). On the other hand, the pressure correction reduces the disagreement in the Clapeyron slope of the postperovskite transition more significantly: from 6.6–13.2 MPa/K to 7.2–10.9 MPa/K. Because of the extreme *P-T* stability of the postperovskite phase, experiments are more challenging and therefore deviatoric stresses, thermal gradients, and compositional gradients may be the importance sources for the discrepancy among the existing studies on the postperovskite transition.

5. Conclusions

1. We measured pressure-volume-temperature data up to 140 GPa and 2500 K for Au+MgO and Pt+MgO mixtures. The mixture samples allow us to compare the equations of state of the three widely used pressure standards at both 300 K and high temperatures for the entire pressure range relevant to the Earth's lower mantle.
2. The use of low shear strength pressure transmitting media together with laser heating enables us to obtain data sets with sufficiently low data scatter (±1 GPa). Owing to the low data scatter, we were able to make precise comparisons of the EOSs at both 300 K and high temperature up to 140 GPa.
3. We optimized the Au, Pt, and MgO scales and made them agree with each other at 300 K up to 135 GPa. Our optimized pressure scales are in agreement with the Au and Pt scales measured in quasi-hydrostatic conditions [*Dewaele et al.*, 2004; *Zha et al.*, 2000] and allow for accurate comparison for data sets based on Au, Pt, and MgO with a ±1 GPa consistency.

4. At high temperature, the Au, Pt, and MgO scales are in agreement with each other within ±1 GPa at pressures between 40 and 130 GPa when the scales by *Dorogokupets and Dewaele* [2007] are used.
5. At high temperature, we found systematic discrepancy among the Au, Pt, and MgO scales at pressures between 20 and 40 GPa with the maximum discrepancy of 3 GPa. The large mismatch at low pressure and high temperature may be due to steep decreases in the Grüneisen parameter, the anharmonicity, and/or the electronic effects in existing EOSs at the pressure range. In order to resolve the disagreement, it is important to (1) develop theories for anharmonic and electronic effects at high pressure and (2) obtain high-resolution elasticity data for a wide range of temperature at 10–40 GPa.
6. Because of its low melting temperature at the pressure range expected for the mantle transition zone and severe anharmonic effects expected at premelting conditions, gold is unsuitable as an internal pressure standard for the determination of the phase boundaries in the mantle transition zone.
7. The use of the scales by *Dorogokupets and Dewaele* [2007] provides tighter constrains for the Clapeyron slopes of the postspinel and postperovskite boundaries. In particular, the postspinel boundary after correction with the scales in *Dorogokupets and Dewaele* [2007] has a boundary slope consistent with seismic estimations for the 660 km discontinuity.
8. For high pressure studies at the *P-T* condition related to the Earth's lower mantle, based on our data, we recommend to use the pressure scales by *Dorogokupets and Dewaele* [2007] at pressures between 40 and 140 GPa at high temperature. However, comparison of results from different pressure scales should be made carefully for the phase boundaries and equations of state of the deep transition zone phases due to the limitations in the existing EOSs for the pressure standards.

Acknowledgments
The discussions with two anonymous reviewers and the Editors have improved the paper. We also thank S. Speziale for discussions. This work is supported by the National Science Foundation (NSF) to S.H.S. (EAR1321976 and EAR1401270). Synchrotron measurements were conducted at the Advanced Photon Source, a U.S. Department of Energy (DOE) Office of Science User Facility operated for the DOE Office of Science by Argonne National Laboratory under contract DE-AC02-06CH11357. X-ray diffraction measurements were performed at GeoSoilEnviroCARS and HPCAT, APS, and ANL. GeoSoilEnviroCARS is supported by the NSF (EAR-1128799) and DOE (DE-FG02-94ER14466). HPCAT is supported by DOE-NNSA (DE-NA0001974) and DOE-BES (DE-FG02-99ER45775). The data for this paper are available by contacting the corresponding author at SHDShim@asu.edu.

References

Bernal, J. D. (1936), Geophysical discussions, *The Observatory*, *59*, 268.
Brown, J. M., and T. J. Shankland (1981), Thermodynamic parameters in the Earth as determined from seismic profiles, *Geophys. J. R. Astron. Soc.*, *66*, 576–596.
Dewaele, A., G. Fiquet, D. Andrault, and D. Häusermann (2000), P-V-T equation of state of periclase from synchrotron radiation measurements, *J. Geophys. Res.*, *105*, 2869–2877.
Dewaele, A., P. Loubeyre, and M. Mezouar (2004), Equations of state of six metals above 94 GPa, *Phys. Rev. B*, *70*, 094112.
Dorfman, S. M., V. B. Prakapenka, Y. Meng, and T. S. Duffy (2012), Intercomparison of pressure standards (Au, Pt, Mo, MgO, NaCl, and Ne) to 2.5 Mbar, *J. Geophys. Res.*, *117*, B08210, doi:10.1029/2012JB009292.
Dorogokupets, P. I., and A. Dewaele (2007), Equation of state of MgO, Au, Pt, NaCl-B1, and NaCl-B2: Internally consistent high-temperature pressure scales, *High Pressure Res.*, *27*, 431–446.
Dorogokupets, P. I., and A. R. Oganov (2007), Ruby, metals, and MgO as alternative pressure scales: A semiempirical description of shock-wave, ultrasonic, x-ray, and thermochemical data at high temperatures and pressures, *Phys. Rev. B*, *75*, 024115.
Dorogokupets, P. I., A. M. Dymshits, T. S. Sokolova, B. S. Danilov, and K. D. Litasov (2015), The equations of state of forsterite, wadsleyite, ringwoodite, akimotoite, $MgSiO_3$-perovskite, and postperovskite and phase diagram for the Mg_2SiO_4 system at pressures of up to 130 GPa, *Russ. Geol. Geophys.*, *56*, 172–189.
Duffy, T. S., and T. J. Ahrens (1995), Compressional sound velocity, equation of state, and constitutive response of shock-compressed magnesium oxide, *J. Geophys. Res.*, *100*, 529–542.
Duffy, T. S., R. J. Hemley, and H.-K. Mao (1995), Equation of state and shear-strength at multimegabar pressures: Magnesium oxide to 227 GPa, *Phys. Rev. Lett.*, *74*, 1371–1374.
Errandonea, D. (2013), High-pressure melting curves of the transition metals Cu, Ni, Pd, and Pt, *Phys. Rev. B*, *87*, 054108.
Fei, Y., H. Li, K. Hirose, W. Minarik, J. Van Orman, W. van Westrenen, T. Komabayashi, and K. Funakoshi (2004a), A critical evaluation of pressure scales at high temperatures by in situ X-ray diffraction measurements, *Phys. Earth Planet. Inter.*, *143–144*, 515–526.
Fei, Y., J. Van Orman, J. Li, W. van Westrenen, C. Sanloup, W. Minarik, K. Hirose, T. Komabayashi, M. Walter, and K. Funakoshi (2004b), Experimentally determined postspinel transformation boundary in Mg_2SiO_4 using MgO as an internal pressure standard and its geophysical implications, *J. Geophys. Res.*, *109*, B02305, doi:10.1029/2003JB002562.
Fei, Y., A. Ricolleau, M. Frank, K. Mibe, G. Shen, and V. Prakapenka (2007), Toward an internally consistent pressure scale, *Proc. Natl. Acad. Sci. U.S.A.*, *104*, 9182–9186.
Golding, B., S. C. Moss, and B. L. Averbach (1967), Composition and pressure dependence of the elastic constants of gold-nickel alloys, *Phys. Rev.*, *158*, 637–646.
Greeff, C. W., and M. J. Graf (2004), Lattice dynamics and the high-pressure equation of state of Au, *Phys. Rev. B*, *69*, 054107.
Hammersley, A. P., (1997), Fit2d: An introduction and overview, *ESRF Internal Rep.*, ESRF.
Hirose, K., S.-I. Karato, V. F. Cormier, J. P. Brodholt, and D. A. Yuen (2006a), Unsolved problems in the lowermost mantle, *Geophys. Res. Lett.*, *33*, L12S01, doi:10.1029/2006GL025691.
Hirose, K., R. Sinmyo, N. Sata, and Y. Ohishi (2006b), Determination of post-perovskite phase transition boundary in $MgSiO_3$ using Au and MgO pressure standards, *Geophys. Res. Lett.*, *33*, L01310, doi:10.1029/2005GL024468.
Hirose, K., N. Sata, T. Komabayashi, and Y. Ohishi (2008), Simultaneous volume measurements of Au and MgO to 140 GPa and thermal equation of state of Au based on the MgO pressure scale, *Phys. Earth Planet. Inter.*, *167*, 149–154.
Holmes, N. C., J. A. Moriarty, G. R. Gathers, and W. J. Nellis (1989), The equation of state of platinum to 660 GPa (6.6 Mbar), *J. Appl. Phys.*, *66*, 2962–2967.
Irifune, T., et al. (1998), The postspinel phase boundary in Mg_2SiO_4 determined by in situ X-ray diffraction, *Science*, *279*, 1698–1700.
Jamieson, J. C., J. N. Fritz, and M. H. Manghnani (1982), Pressure measurement at high temperature in X-ray diffraction studies: Gold as a primary standard, in *High-Pressure Research in Geophysics*, edited by S. Akimoto and M. H. Manghnani, pp. 27–48, Cent. for Acad. Publ. Jpn., Tokyo.

Karki, B. B., and L. Stixrude (1999), Seismic velocities of major silicate and oxide phases of the lower mantle, *J. Geophys. Res.*, *104*, 13,025–13,033.
Katsura, T., et al. (2003), Post-spinel transition in Mg_2SiO_4 determined by high P–T in situ X-ray diffractometry, *Phys. Earth Planet. Inter.*, *136*, 11–24.
Kennett, B. L. N., and I. Jackson (2009), Optimal equations of state for mantle minerals from simultaneous non-linear inversion of multiple datasets, *Phys. Earth Planet. Inter.*, *176*, 98–108.
Kono, Y., T. Irifune, Y. Higo, T. Inoue, A. Barnhoorn, D. Suetsugu, C. Bina, D. Wiens, and M. Jellinek (2010), $P-V-T$ relation of MgO derived by simultaneous elastic wave velocity and in situ X-ray measurements: A new pressure scale for the mantle transition region, *Phys. Earth Planet. Inter.*, *183*, 196–211.
Lebedev, S., S. Chevrot, and R. van der Hilst (2002), Seismic evidence for olivine phase changes at the 410- and 660-kilometer discontinuities, *Science*, *296*, 1300–1302.
Li, B., K. Woody, and J. Kung (2006), Elasticity of MgO to 11 GPa with an independent absolute pressure scale: Implications for pressure calibration, *J. Geophys. Res.*, *111*, B11206, doi:10.1029/2005JB004251.
Litasov, K., and E. Ohtani (2002), Phase relations and melt compositions in CMAS–pyrolite–H_2O system up to 25 GPa, *Phys. Earth Planet. Inter.*, *134*, 105–127.
Matsui, M., E. Ito, T. Katsura, D. Yamazaki, T. Yoshino, A. Yokoyama, and K. Funakoshi (2009), The temperature-pressure-volume equation of state of platinum, *J. Appl. Phys.*, *105*, 013505.
Menéndez-Proupin, E., and A. K. Singh (2007), Ab initio calculations of elastic properties of compressed Pt, *Phys. Rev. B*, *76*, 054117.
Meng, Y., G. Shen, and H. K. Mao (2006), Double-sided laser heating system at HPCAT for in situ x-ray differentiation at high pressures and high temperatures, *J. Phys. Condens. Matter*, *18*, S1097—S1103.
Oganov, A. R., and P. I. Dorogokupets (2003), All-electron and pseudopotential study of MgO: Equation of state, anharmonicity, and stability, *Phys. Rev. B*, *67*, 224110.
Ono, S., and A. R. Oganov (2005), In situ observations of phase transition between perovskite and $CaIrO_3$-type phase in $MgSiO_3$ and pyrolitic mantle composition, *Earth Planet. Sci. Lett.*, *236*, 914–932.
Ono, S., J. P. Brodholt, and G. D. Price (2011), Elastic, thermal and structural properties of platinum, *J. Phys. Chem. Solids*, *72*, 169–175.
Prakapenka, V. B., A. Kubo, A. Kuznetsov, A. Laskin, O. Shkurikhin, P. Dera, M. L. Rivers, and S. R. Sutton (2008), Advanced flat top laser heating system for high pressure research at GSECARS: Application to the melting behavior of germanium, *High Pressure Res.*, *28*, 225–235.
Rivers, M., V. B. Prakapenka, A. Kubo, C. Pullins, C. M. Holl, and S. D. Jacobsen (2008), The COMPRES/GSECARS gas-loading system for diamond anvil cells at the advanced photon source, *High Pressure Res.*, *28*, 273–292.
Shim, S.-H. (2008), The postperovskite transition, *Annu. Rev. Earth Planet Sci.*, *36*, 569–599.
Shim, S.-H., T. S. Duffy, and G. Shen (2001), The post-spinel transformation in $Mg_2SiO_4$and its relation to the 660-km seismic discontinuity, *Nature*, *411*, 571–574.
Shim, S.-H., T. S. Duffy, and K. Takemura (2002), Equation of state of gold and its application to the phase boundaries near the 660-km depth in the mantle, *Earth Planet. Sci. Lett.*, *203*, 729–739.
Singh, A. K. (1993), The lattice strains in a specimen (cubic system) compressed nonhydrostatically in an opposed anvil device, *J. Appl. Phys.*, *73*, 4278–4286.
Singh, A. K., and K. Takemura (2001), Measurement and analysis of nonhydrostatic lattice strain component in niobium to 145 GPa under various fluid pressure-transmitting media, *J. Appl. Phys.*, *90*, 3269–3275.
Singh, A. K., H.-K. Mao, J. Shu, and R. J. Hemley (1998), Estimation of single-crystal elastic moduli from polycrystalline X-ray diffraction at high pressure: Application to FeO and iron, *Phys. Rev. Lett.*, *80*, 2157–2160.
Sokolova, T. S., P. I. Dorogokupets, and K. D. Litasov (2013), Self-consistent pressure scales based on the equations of state for ruby, diamond, MgO, B2–NaCl, as well as Au, Pt, and other metals to 4 Mbar and 3000 K, *Russ. Geol. Geophys.*, *54*, 181–199.
Speziale, S., C.-S. Zha, T. S. Duffy, R. J. Hemley, and H.-K. Mao (2001), Quasi-hydrostatic compression of magnesium oxide to 52 GPa: Implications for the pressure-volume-temperature equations of state, *J. Geophys. Res.*, *106*, 515–528.
Takemura, K. (2001), Evaluation of the hydrostaticity of a helium-pressure medium with powder X-ray diffraction techniques, *J. Appl. Phys.*, *89*, 662–668.
Takemura, K., and A. Dewaele (2008), Isothermal equation of state for gold with a He-pressure medium, *Phys. Rev. B*, *78*, 104119.
Tange, Y., E. Takahashi, Y. Nishihara, K. Funakoshi, and N. Sata (2009), Phase relations in the system MgO-FeO-SiO_2 to 50 GPa and 2000°C: An application of experimental techniques using multianvil apparatus with sintered diamond anvils, *J. Geophys. Res.*, *114*, B02214, doi:10.1029/2008JB005891.
Tateno, S., K. Hirose, N. Sata, and Y. Ohishi (2009), Determination of post-perovskite phase transition boundary up to 4400 K and implications for thermal structure in D″ layer, *Earth Planet. Sci. Lett.*, *277*, 130–136, doi:10.1016/j.epsl.2008.10.004.
Tsuchiya, T. (2003), First-principles prediction of the $P-V-T$ equation of state of gold and the 660-km discontinuity in Earth's mantle, *J. Geophys. Res.*, *108*, 2462.
Tsuchiya, T., and K. Kawamura (2002), First-principles electronic thermal pressure of metal Au and Pt, *Phys. Rev. B*, *66*, 094115.
Vinet, P., J. Ferrante, J. H. Rose, and J. R. Smith (1987), Compressibility of solids, *J. Geophys. Res.*, *92*, 9319–9325.
Weidner, D. J., Y. Wang, and M. T. Vaughan (1994), Yield strength at high pressure and temperature, *Geophys. Res. Lett.*, *21*, 753–756.
Wu, Z., R. M. Wentzcovitch, K. Umemoto, B. Li, K. Hirose, and J.-C. Zheng (2008), Pressure-volume-temperature relations in MgO: An ultrahigh pressure-temperature scale for planetary sciences applications, *J. Geophys. Res.*, *113*, B06204.
Ye, Y., C. Gu, S.-H. Shim, Y. Meng, and Y. Prakapenka (2014), The postspinel boundary in pyrolitic compositions determined in the laser-heated diamond anvil cell, *Geophys. Res. Lett.*, *41*, 3833–3841, doi:10.1002/2014GL060060.
Yokoo, M., N. Kawai, K. G. Nakamura, and K. i. Kondo (2009), Ultrahigh-pressure scales for gold and platinum at pressures up to 550 GPa, *Phys. Rev. B*, *80*, 104114.
Zha, C. S., H.-K. Mao, and R. J. Hemley (2000), Elasticity of MgO and a primary pressure scale to 55 GPa, *Proc. Natl. Acad. Sci. U.S.A.*, *97*, 13,494–13,499.
Zha, C.-S., K. Mibe, W. A. Bassett, O. Tschauner, H.-K. Mao, and R. J. Hemley (2008), $P-V-T$ equation of state of platinum to 80 GPa and 1900 K from internal resistive heating/x-ray diffraction measurements, *J. Appl. Phys.*, *103*, 054908.
Zhang, L., and Y. Fei (2008), Melting behavior of (Mg, Fe)O solid solutions at high pressure, *Geophys. Res. Lett.*, *35*, L13302, doi:10.1029/2008GL034585.
Zhuravlev, K. K., A. F. Goncharov, S. N. Tkachev, P. Dera, and V. B. Prakapenka (2013), Vibrational, elastic, and structural properties of cubic silicon carbide under pressure up to 75 GPa: Implication for a primary pressure scale, *J. Appl. Phys.*, *113*, 113503.

Erratum

In the originally published version of this article, Data Sets S1 through S4 contained rounded numbers. The files have been updated, and this version may be considered the authoritative version of record.